Nuclear Magnetic Resonance Structural Studies of a Potassium Channel−Charybdotoxin Complex‡

Liping Yu,§ Chaohong Sun,§ Danying Song, Jianwei Shen, Nan Xu, Angelo Gunasekera, Philip J. Hajduk, and Edward T. Olejniczak*

Pharmaceutical Discovery Division, GPRD, Abbott Laboratories, Abbott Park, Illinois 60064-6098

Received August 19, 2005; Revised Manuscript Received October 3, 2005

ABSTRACT: Ion channels play critical roles in signaling processes and are attractive targets for treating various diseases. Here we describe an NMR-based strategy for structural analyses of potassium channel−ligand complexes using KcsA (residues 1−132, with six mutations to impart toxin binding and to mimic the eukaryotic hERG channel). Using this approach, we determined the solution structure of KcsA in complex with the high-affinity peptide antagonist charybdotoxin. The structural data reveal how charybdotoxin binds to the closed form of KcsA and makes specific contacts with the extracellular surface of the ion channel, resulting in pore blockage. This represents the first direct structural information about an ion channel complexed to a peptide antagonist and provides an experimental framework for understanding and interpreting earlier mutational analyses. The strategy presented here overcomes many of the limitations of conventional NMR approaches to helical membrane protein structure determination and can be applied in the study of the binding of druglike molecules to this important class of proteins.

Potassium channels play critical roles in vital cellular signaling processes regulating neuronal and cardiac electrical functions, neurotransmitter release, and propagation of action potential. Recent genetic linkage analyses have found that many cardiac, neuronal, and renal diseases are associated with the malfunction of potassium channels, making them potential therapeutic targets for a variety of indications (*1*). However, despite intense therapeutic interest, the tools of structural biology and structure-based drug design have not played a significant role in discovery efforts against ion channels. While recent breakthroughs in X-ray crystallography have revealed the three-dimensional structures of several potassium channels in both the closed and open forms (*2*−*6*), obtaining the structures of ion channels in complex with either endogenous or xenobiotic antagonists has remained difficult.

Over the past few decades, NMR spectroscopy has emerged as a powerful tool for the high-resolution structure determination of proteins and protein−ligand complexes. However, conventional NMR assignment strategies that rely on amide resonances may not be applicable to many helical membrane proteins. While the NMR structures of two low-molecular weight helical membrane proteins have been described (*7*, *8*) and progress has been reported in the backbone assignment of at least two other helical membrane proteins (*9*, *10*), the high mobility of the transmembrane helices can often lead to extensive broadening of the amide proton signals (*11*). In contrast, the resonances of side chain methyl groups are less sensitive to these effects. As a result, alternative strategies for structural analyses employing sparse NOE data have been proposed (*12*−*14*). However, all of these methods currently rely on either backbone amide resonances or protein structures complexed to known reference ligands to guide the methyl group assignments, neither of which is available for ion channel complexes.

Here we present the first direct structural information about a surrogate KcsA ion channel complexed to the high-affinity peptide antagonist charybdotoxin using an NMR-based approach that relies solely on side chain methyl and aromatic resonances and obviates the need for backbone amide resonance assignment. The solution structure described here is consistent with previously reported mutational data and provides structural insight into the energetics that govern high-affinity binding of charybdotoxin to the ion channel. Moreover, the approach is generalizable and can potentially be applied to the study of potassium channels or other integral membrane protein systems of known structure complexed to small molecule modulators.

EXPERIMENTAL PROCEDURES

Cloning and Protein Preparation. KcsA (residues 1−132) (GenBank accession code Q54397) with six mutations (Q58A, T61S, R64D, F103Y, T107F, and L110V) was cloned into the pIVEX-2.4d vector (Roche Applied Science) and expressed in C41(DE3) cells (Avidis). The resulting proteins contain 23 additional residues (MSGSHHHHHH-SSGIEGRGRLIKH) at the N-terminus of KcsA. Site-directed mutants were prepared using the QuikChange mutagenesis kit (Stratagene). A total of 14 mutants were made for

‡ The average minimized coordinates for the KcsA−charybdotoxin complex have been deposited with the Protein Data Bank (PDB entry 2A9H). The methyl group assignments obtained for the free KcsA have been deposited with the BioMagResBank database (entry BMRB-13262).

* To whom correspondence should be addressed: Abbott Laboratories, R46Y, AP-10, 100 Abbott Park Rd., Abbott Park, IL 60064-3500. Phone: (847) 937-0298. Fax: (847) 938-2478. E-mail: Edward.olejniczak@abbott.com.

§ These authors contributed equally to this work.

10.1021/bi051656d CCC: $30.25
Published on Web 11/02/2005

assignments (L24I, L36I, L40I, A57G, L66I, V84I, L86I, V91I, L93I, V95I, L97I, L105I, V106I, and V110I), and seven additional mutants (A58F, A58G, L81A, L81W, Y82A, Y82L, and Y82F) were prepared to probe the energetics of toxin binding.

Proteins were purified using a previously described protocol (*15*) with minor modifications. After the high-speed ultracentrifugation, 25 mM Foscholine-12 (Anatrace) was used to extract the protein from the membrane. The protein was purified to homogeneity through a Ni−NTA column (Qiagen) followed by gel filtration on a Superdex-75 column (Pharmacia), with a protein elution time consistent with the formation of a tetramer. The melting temperature (T_M) for tetramer formation was determined by incubating the purified protein for 15 min at various temperatures (ranging from 298 to 368 K) and visualizing the monomer−tetramer equilibrium on a 0.1% SDS gel. Charybdotoxin was purchased from Bachem and used without further purification.

Assessment of Charybdotoxin Binding. Dissociation constants between charybdotoxin and the various KcsA mutants were performed in a buffer containing 20 mM sodium phosphate (pH 7.5), 5 mM KCl, 1 mM DTT, and 5 mM Foscholine-12. Six samples containing charybdotoxin at 0.5 μM and KcsA at concentrations ranging from 0.1 to 30 μM were passed through a 30 kDa membrane filter (Pall), and the flow-through was analyzed by mass spectroscopy to determine the fraction of charybdotoxin not retained by KcsA. A control peptide was added to each sample before injection to serve as an internal intensity standard. LC−MS analyses were performed using a Thermo Finnigan LCQ-DECA ion trap mass spectrometer equipped with a standard electrospray ionization (ESI) source and a Waters 2690 HPLC system. The mass intensities were converted into the fraction of peptide retained, and the resulting data were fit to a single-binding site equilibrium equation to yield the final dissociation constants. Six points were analyzed (half-log dilutions) in duplicate for each sample.

NMR Spectroscopy. Uniformly ^{15}N-labeled samples with selectively ^{13}C-labeled protonated methyl groups of either {IVL}, {VL}, or {IVLMA} in a ^{2}H background were prepared by growing cells in media that contained 100% $^{2}H_2O$ [Cambridge Isotope Laboratories (CIL) and Isotec], D-glucose-d_{12} (3 g/L, CIL and Isotec), and $^{15}NH_4Cl$ (1 g/L, CIL and Isotec), and by supplementing media with a combination of either [3-^{13}C]-α-ketobutyrate (50 mg/L, for labeling isoleucine methyl groups), [3,3-$^{13}C_2$]-α-ketoisovalerate (100 mg/L, for labeling valine and leucine methyl groups simultaneously), $^{13}C_\epsilon H_3$-labeled Met (100 mg/L, CIL), or $^{13}C_\beta H_3$-labeled Ala (100 mg/L, CIL). The $^{13}CH_3${LA} sample was prepared by supplementing the media with [U-$^{13}C_6$,^{15}N]leucine (100 mg/L, CIL) and $^{13}C_\beta H_3$-labeled Ala (100 mg/L, CIL). The $^{13}CH_3${IVLMA}/^{1}H{YW} sample was prepared in a manner similar to that for the $^{13}CH_3${IVLMA} sample except the medium was supplemented with [U-$^{13}C_9$]-Tyr (100 mg/L, CIL) and protonated Trp (100 mg/L, Sigma). Under these growth conditions, a high level of incorporation of all labeled side chains was observed with limited scrambling (as illustrated in Figure S1 of the Supporting Information for the $^{13}CH_3${LA} sample).

NMR samples contained 1 mM KcsA and/or 0.25 mM charybdotoxin in 20 mM sodium phosphate (pH 7.5), 5 mM KCl, 1 mM DTT, and 80 mM Foscholine-12-d_{38} (Cambridge). NMR spectra were recorded at 42 °C on Bruker DRX600 or DRX800 NMR spectrometers. Three-dimensional ^{1}H−^{13}C-resolved NOESY spectra were acquired for KcsA in the presence and absence of charybdotoxin using mixing times of 80−100 ms. Assignments for free toxin were obtained using two-dimensional ^{1}H−^{1}H NOESY (mixing times of 100−150 ms) and ^{1}H−^{1}H TOCSY (mixing times of 25−38 ms) spectra in the same detergent solvent system as the final complex [20 mM sodium phosphate (pH 7.5), 5 mM KCl, 1 mM DTT, and 80 mM Foscholine-12-d_{38}]. Assignments for bound toxin were obtained using two-dimensional ^{1}H−^{1}H NOESY (mixing times of 100−150 ms) spectra on charybdotoxin in the presence of perdeuterated KcsA. Sample regions of the ^{1}H−^{1}H NOESY spectra of charybdotoxin in the presence and absence of KcsA are given in the Supporting Information (Figure S2).

Structure Calculations. For the KcsA−charybdotoxin complex, the structure calculations were performed in CNX (*16*) using a HADDOCK-type protocol (*17*) comprised of (1) rigid body docking starting from the unbound structures of KcsA (PDB entry 1BL8) (*2*) and charybdotoxin (PDB entry 2CRD) (*18*) using restraints from the intermolecular NOE data, (2) high-temperature (1000 K) simulated annealing, and (3) molecular dynamics (2 ns, 300 K) using explicit water solvation and full electrostatics. NOE-derived distance restraints had upper bounds of 3.0, 4.0, and 5.0 Å. A total of 452 (113 × 4) distance restraints derived from KcsA−KcsA NOEs, 111 restraints derived from toxin−toxin NOEs, noncrystallographic symmetry (NCS) restraints in the helical regions for KcsA, and a total of 13 KcsA−charybdotoxin intermolecular NOE restraints were used in the calculations. Intrasubunit and intersubunit NOEs for KcsA were distinguished on the basis of inspection of the X-ray crystal structure. NOEs between toxin and KcsA were implemented as ambiguous with respect to the KcsA subunits. As the methyl−methyl and methyl−aromatic NOEs were consistent with the reported secondary structure of KcsA, the helices were maintained with dihedral restraints on residues 24−52, 64−73, and 86−115 of KcsA and residues 10−20 of the toxin. In addition, only a single resonance signal was observed for the assigned methyl residues of KcsA in these three helical regions (Figure 1), indicating that *C*4 symmetry is maintained. This was incorporated in the calculations by using noncrystallographic symmetry equivalence for these three helical regions in CNX (*16*).

RESULTS AND DISCUSSION

NMR Assignments of KcsA. Potassium channels are remarkably conserved in the three-dimensional structures of the tetrameric pore-forming domain. This domain contains two transmembrane helices (M1 and M2, corresponding to S5 and S6, respectively, of eukaryotic voltage-gated potassium channels) and a pore (P) region. The bacterial protein KcsA contains the minimal structural requirements for a potassium channel. Starting from KcsA, we constructed a surrogate channel (see Figure 1) in which key amino acids were mutated to impart toxin binding by mimicking critical residues of the eukaryotic Shaker channel (Q58A, T61S, and R64D) (*19*) and to mimic the central cavity of the eukaryotic HERG channel (F103Y, T107F, and L110V) (*20*), while maintaining high expression levels of the functionally intact protein. The resulting construct forms a highly stable tetramer

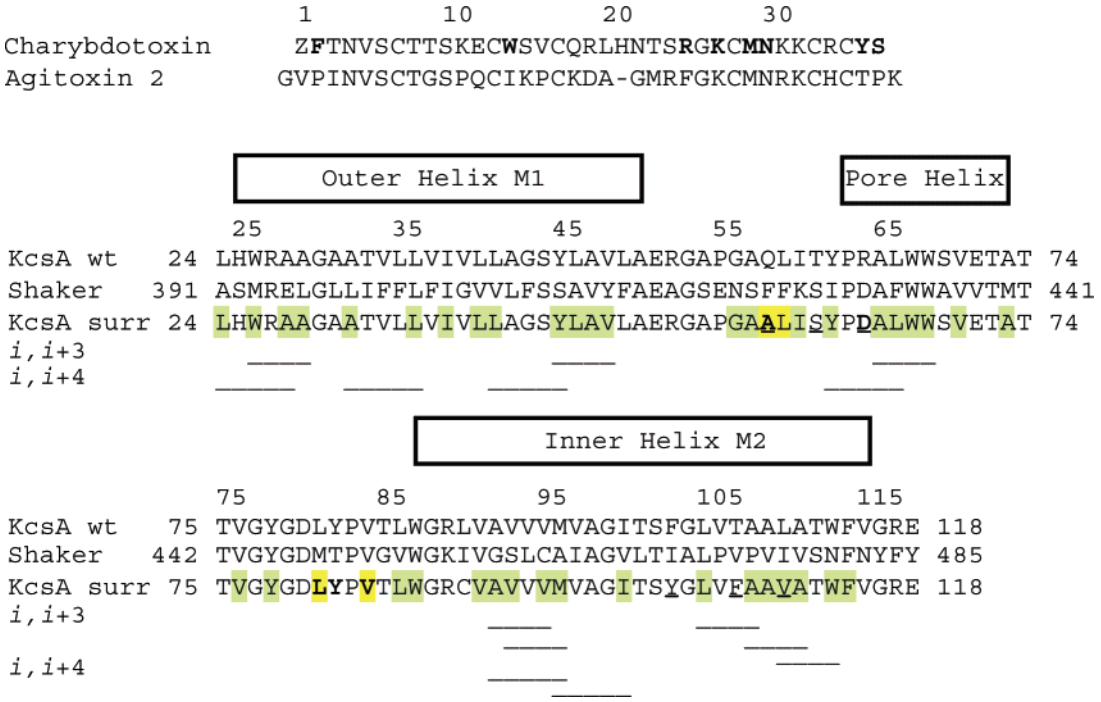

FIGURE 1: Sequence alignment of charybdotoxin and agitoxin 2 (top) and wild-type KcsA (KcsA wt), the surrogate KcsA used in this study (KcsA surr), and the *Shaker* K^+ channels (bottom). Residues in KcsA that were mutated to impart toxin binding and mimic the central cavity of HERG are underlined. Assigned residues that exhibit only a single resonance in the presence of toxin (indicating that *C*4 symmetry is maintained) are highlighted in green, while those that split into more than one peak (indicating that *C*4 symmetry is broken) are highlighted in yellow. Selected residues shown in bold in either charybdotoxin or KcsA are involved in the interaction interface as described in the text. Bars at the bottom of the sequence indicate helical NOE contacts observed between side chains of residues separated by one helical turn.

(T_M ~ 85 °C in 0.1% SDS) with expression levels of ~7 mg/L on minimal media.

Despite the availability of highly deuterated and isotopically labeled protein, conventional or TROSY-based strategies for backbone resonance assignments for this protein were unsuccessful due to short transverse relaxation times and incomplete back-exchange of the amide protons. In contrast, as shown in Figure 2, high-resolution $^1H-^{13}C$ HSQC spectra can be obtained for the methyl groups of this protein, enabling screening and structural analyses using sparse NOE data (*12*−*14*). To assign the methyl groups of the protein, an assignment strategy based on site-directed mutagenesis and multiple selectively labeled samples was employed. As illustrated in Figure 2, the L86I mutation causes two leucine methyl resonances to disappear and a new Ile Cδ1 resonance to appear in the spectra, leading to the assignment of the two L86 methyl groups. This approach was used for the assignment of 12 methyl-containing amino acids via comparison of the NMR spectra of the parent and mutant proteins.

Additional assignments were obtained in the context of the known structure by analysis and comparison of three-dimensional (3D) ^{13}C-edited NOESY spectra acquired on four selectively $^{13}CH_3$-labeled samples as well as a sample containing protonated methyl groups and the aromatic amino acids tyrosine and tryptophan. For example, a comparison of the 3D $^1H-^{13}C$ NOESY spectra for the perdeuterated $^{13}CH_3${IVL}, $^{13}CH_3${LA}, and $^{13}CH_3${VL} samples allowed for the unambiguous assignment of the valine, leucine, isoleucine, and alanine resonances by residue type. $^1H-^{13}C$ NOESY spectra for the perdeuterated $^{13}CH_3${IVLMA} and $^{13}CH_3${IVLMA}/^1H{YW} samples were then analyzed to follow NOE connectivities throughout the methyl and aromatic spins using the unambiguous mutant-derived assignments as anchor points. In total, 73% of the methyl groups of valine, leucine, isoleucine, alanine, and methionine and 80% of the aromatic side chains of tryptophan and tyrosine were assigned for residues 20−120 of KcsA (see Figure 1 and Figure S1).

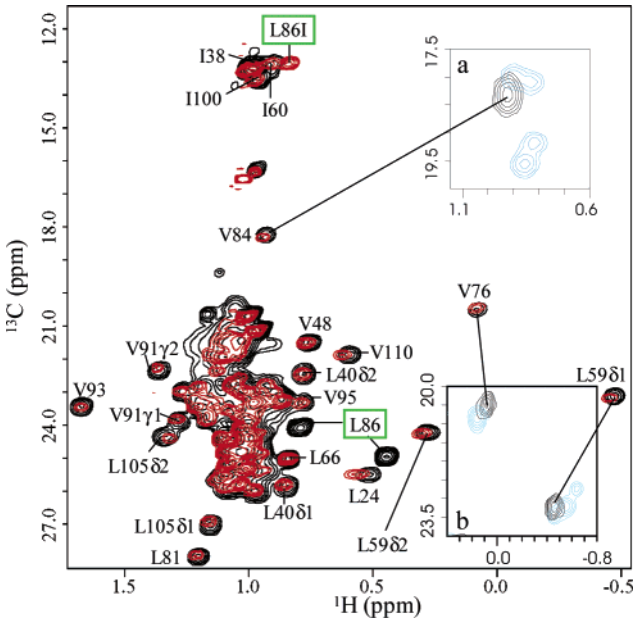

FIGURE 2: Regions of $^{13}C-^1H$ HSQC spectra acquired on perdeuterated, $^{13}CH_3${IVL}-labeled KcsA. Shown are spectra for the parent (black), L86I mutant (red), and parent protein in the presence of charybdotoxin (blue, insets). Assignments for selected cross-peaks are indicated. Assignment labels for L86 and the isoleucine mutant (L86I) are boxed in green. Stereospecific methyl group assignments were not obtained.

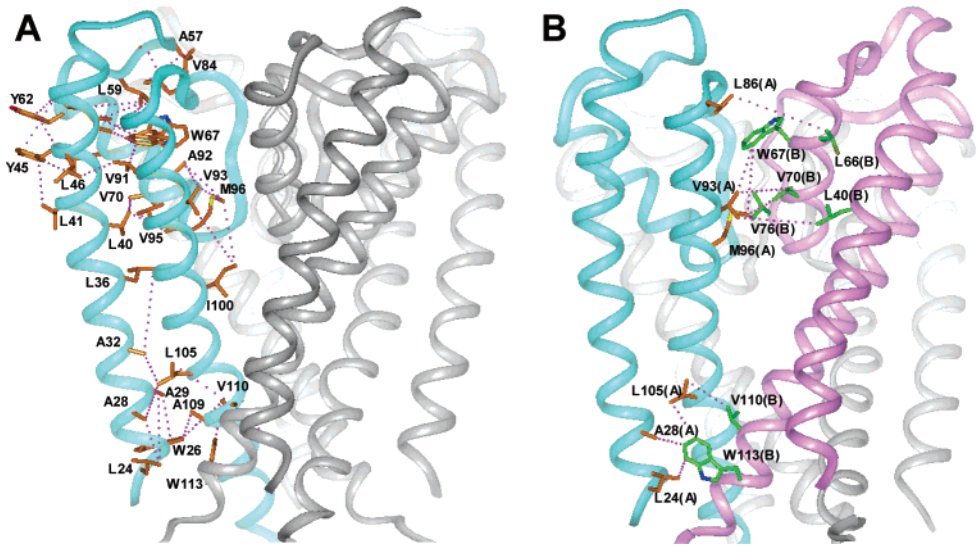

FIGURE 3: Summary of (A) intramonomer and (B) intermonomer NOE contacts for KcsA. (A) NOE contacts for only one KcsA monomer (colored cyan) are shown. (B) Intermonomer contacts for only one pair of KcsA monomers (colored cyan and magenta) are shown. Residues of KcsA involved in NOE contacts are rendered as sticks, and the NOE contacts themselves are shown as dotted lines. For clarity, the NOE contacts are not shown regiospecifically (e.g., no distinction was made between stereospecific methyl or aromatic protons).

Solution Structure of KcsA. The crystal structure of KcsA exhibits a tetrameric arrangement of the helical KcsA monomers that provides the structural basis for ion permeation and K^+ selectivity (*2*). While structures of potassium channels have been determined for both the closed and open forms (*21*), KcsA exists in the closed form in the crystalline state. The conformation of KcsA in solution was characterized with our NMR data. For our KcsA construct, the side chain NOE data are clearly consistent with the reported helical secondary structure for KcsA, as numerous NOEs are observed between the side chains of residues separated by one helical turn (e.g., i to $i + 3$ or $i + 4$ contacts) (see Figure 1). In addition, the tertiary arrangement of the helices within each KcsA monomer is indistinguishable from the crystal structure. For example, as shown in Figure 3A, long-range intramonomer NOEs unambiguously define the packing of the pore helix onto the M1 and M2 helices, while additional long-range NOEs define the intracellular arrangement of the terminal ends of the M1 and M2 helices. Furthermore, as shown in Figure 3B, intermonomer NOEs at both the pore and the intracellular gate indicate a quaternary arrangement consistent with the crystal structure. In particular, the NOEs between residues L24, A28, and L105 on one monomer and V110 and W113 on an adjacent monomer in the intracellular gate region (see Figure 3B) indicate that the channel is in the closed conformation in solution. Finally, since only one set of resonances is observed for each monomer, the symmetry of the tetrameric ion channel is also unambiguous. Thus, the NMR data indicate that the solution conformation of our KcsA construct is the same as that reported previously by X-ray methods. While it has been reported that channel gating can occur more frequently at low pH in lipid bilayer systems (*22*), no spectral changes were observed for KcsA at pH values as low as 4.5 (data not shown), indicating that even at low pH the channel remains in the closed conformation.

Solution Structure of the KcsA−Charybdotoxin Complex. Scorpion toxins bind with high affinity to eukaryotic potassium channels and are widely used as probes of potassium channel structure and function. To date, the only available structural information about the bound complex has been indirect proximity information derived from mutational analyses (*23*−*26*), cross saturation experiments (*27*), and docking simulations (*28*, *29*). However, ambiguities and discrepancies in some of the experimental data have led to differences in the proposed docking models (*30*).

Using a filter binding assay (see Experimental Procedures), we have determined a K_D value of 900 nM for binding of charybdotoxin to our surrogate KcsA, which is very similar to the value reported earlier for agitoxin 2 (K_D 620 nM) binding to a similar KcsA construct (*19*, *27*). When charybdotoxin is added to KcsA, the majority of the cross-peaks in the NMR spectra exhibit only a single resonance, indicating that *C*4 symmetry is maintained for most of the tetramer. In contrast, as shown in the insets of Figure 2, the *C*4 symmetry for residues at or near the binding interface is broken, resulting in four distinct cross-peaks for the residues on each of the four monomeric subunits. Saturation of the chemical shift perturbations of the KcsA resonances was observed at a 1:4 toxin:KcsA ratio, consistent with binding of one toxin molecule per KcsA tetramer. As shown in Figure 4, distinct intermolecular NOE patterns can be observed for each of the monomer-specific resonances involved in binding of toxin.

From an analysis of the NMR data, a total of 13 intermolecular distance restraints were obtained between toxin and methyl-containing amino acids on KcsA (see Figure 5A), along with 563 intramolecular distance restraints and the noncrystallographic symmetry restraints. Structure calculations starting from the unbound structures of KcsA and charybdotoxin resulted in a single low-energy conformation for the KcsA−charybdotoxin complex. The resulting structures had no NOE penalties greater than 0.3 Å, with a final ensemble exhibiting an rmsd of 0.66 ± 0.05 Å for all backbone atoms (N, Cα, and C′) and 0.92 ± 0.05 Å for all heavy atoms in the complex (see Table S1). The rmsd values for charybdotoxin are 1.35 ± 0.26 Å for all backbone atoms (N, Cα, and C′) and 1.69 ± 0.27 Å for all heavy atoms when the backbone of the complex was superimposed (see Table S1 and Figure S3 of the Supporting Information).

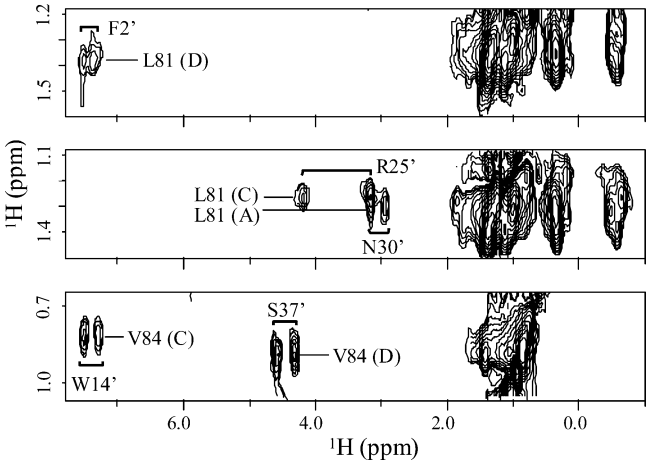

FIGURE 4: Slices from a ^{13}C-resolved NOESY experiment acquired on perdeuterated, $^{13}CH_3${IVL}-labeled KcsA in complex with charybdotoxin. Individual KcsA monomers are given in parentheses, while toxin residues are indicated with a prime.

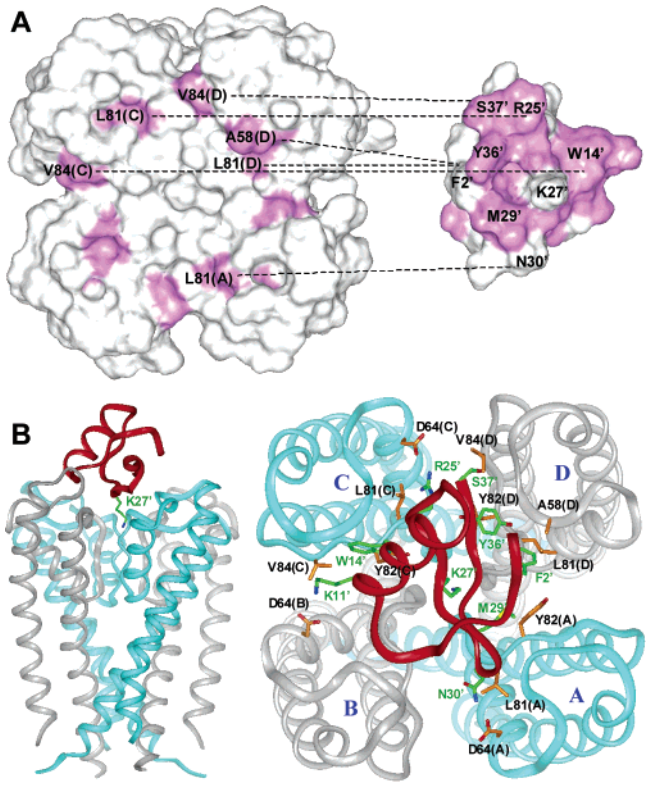

FIGURE 5: (A) Binding interfaces of the potassium ion channel KcsA and charybdotoxin as determined by NOE contacts and chemical shift perturbations. Direct NOE contacts between specified residues are indicated by dashed lines. Residues exhibiting a weighted chemical shift perturbation $\{\Delta = [\Delta(^1H)^2 + \Delta(^{13}C)^2/5]^{0.5}\}$ greater than 0.15 ppm are colored pink. (B) Ribbon plots depicting the average, minimized structure of KcsA (cyan and gray ribbons) complexed to charybdotoxin (red ribbon). Side and top views (relative to the channel) are shown at the left and right, respectively. Selected side chains are rendered as sticks with green and orange carbon atoms for charybdotoxin and KcsA, respectively. The four subunits of KcsA are labeled A−D.

The toxin-bound structure of KcsA remains in the closed conformation, and only minor conformational changes in the extracellular loops are necessary for accommodation of complex formation. In addition, the bound structure of charybdotoxin is very similar to that of the peptide free in solution (*18*). The intermolecular NOEs observed between

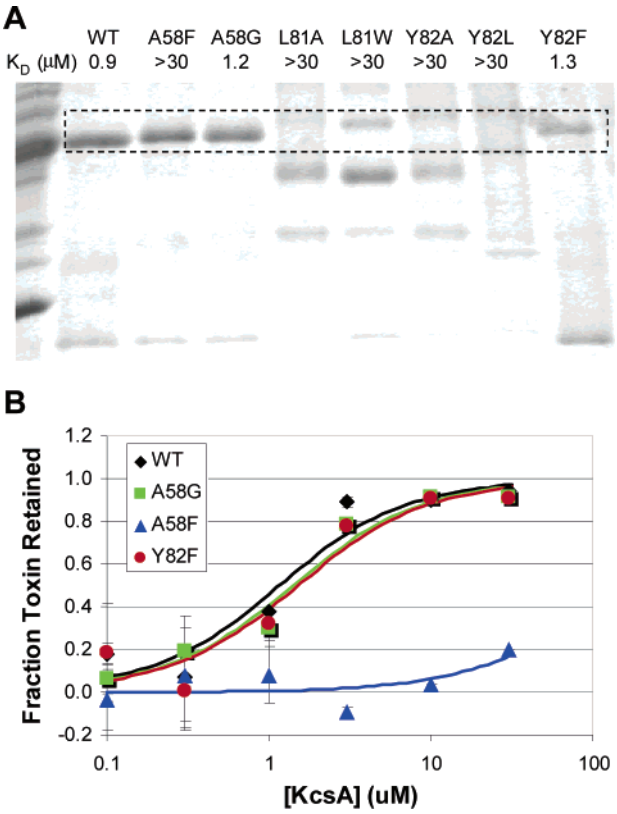

FIGURE 6: (A) SDS gel (0.1%) of the KcsA surrogate described in this work (WT) along with seven site-directed mutants. The loading samples were nonboiled, and the location of the tetramer band is indicated by the dashed box. All samples were >90% pure, so the laddering effect observed for L81A, L81W, Y82A, and Y82L is an indication of a mixture of monomer, dimer, trimer, and tetramer forms under these conditions. The measured K_D values for charybdotoxin are given under the mutant identifier. (B) Titration curves from the filter binding assay for binding of charybdotoxin to the parent KcsA construct (WT, black diamonds) and mutants A58G (green squares), A58F (blue triangles), and Y82F (red circles). Duplicates were obtained for each point, and the error bars represent the standard deviations. The solid lines correspond to the fitted K_D values.

KcsA and charybdotoxin unambiguously orient the toxin on the extracellular side of KcsA and result in the insertion of the side chain of K27′ directly into the pore. For example, residue L81 of KcsA on monomer units A [L81(A)], C [L81(C)], and D [L81(D)] exhibits distinct NOEs to toxin residues N30′ (toxin residues are denoted with a prime), R25′, and F2′, respectively (Figures 4 and 5). Similarly, V84(C) and V84(D) exhibit NOEs to residues W14′ and S37′, respectively. A58(D) also exhibits an NOE to F2′. From the complexed structure, Y82(A) is in hydrophobic contact with M29′, while Y82(D) forms a stacking interaction with Y36′, consistent with the large chemical shift perturbations observed for M29′ and Y36′ upon binding to KcsA. The structural data thus clearly define how the toxin binds to the channel and blocks K^+ ion entry.

Structure-Based Mutations of KcsA. On the basis of the NMR solution structure, mutations were made in KcsA to assess the energetic contribution of key residues to charybdotoxin binding. As shown in Figure 6, seven site-directed mutants involving residues A58, L81, and Y82 were prepared and analyzed for both tetramer stability and toxin binding. While the methyl group of A58 forms a contact with F2′ of toxin (see Figure 5), mutation of this residue to a glycine

(A58G) has no effect on toxin binding. However, mutation to a bulky phenylalanine group (A58F) completely abrogates binding, consistent with a steric clash between the mutated side chain and F2′ of toxin. Residue Y82 from several monomer units of KcsA makes interactions with multiple residues on charybdotoxin, including M29′ and Y36′ (see Figure 5). Mutation of this residue to a phenylalanine (Y82F) also has no effect on toxin binding, indicating that the hydroxyl group on Y82 does not substantially contribute to the binding affinity. Mutation of Y82 to either alanine (Y82A) or leucine (Y82L) completely abolishes binding to toxin. However, unlike the A58G, A58F, and Y82F mutations, Y82A and Y82L exhibit reduced tetramer stability compared to the parent construct when visualized on a 0.1% SDS gel (see Figure 6A). As Y82 is located at the intersubunit interface, it is not surprising that significant modifications of this residue would perturb subunit contacts. Thus, while the structural and mutational data clearly indicate a substantial role for Y82 in toxin binding, a quantitative estimate for the contribution to the binding affinity is complicated by the energetics associated with tetramer formation. Similar arguments can be made for mutations in L81 (L81A and L81W), both of which completely abrogate toxin binding but also reduce tetramer stability (Figure 6A).

Comparison to Previous Mutational Analyses. Apart from the mutants described above, little else is known about the specific residues on KcsA that are required for toxin binding. However, extensive mutational analyses have been reported for the *Shaker* K^+ channel in an effort to identify residues involved in toxin binding (*23*−*25*). Significantly, all of the residues of KcsA that exhibit NOEs to charybdotoxin have corresponding residues in *Shaker* that are critical for high-affinity charybdotoxin binding. A58 of KcsA corresponds to F425 of the *Shaker* K^+ channel (see Figure 1). Mutation of this residue to a glycine *increases* the affinity of charybdotoxin for the *Shaker* channel by 1900-fold (*23*, *31*), suggesting that even in *Shaker* the native phenylalanine side chain makes an energetically unfavorable contact with the toxin. L81 and V84 of KcsA correspond to M448 and V451 of *Shaker*, respectively, both of which exhibit >800-fold decreases in affinity for charybdotoxin when they are mutated to lysines. D64 and Y82 of KcsA correspond to D431 and T449 of *Shaker*, respectively, and are also implicated by both the structural and mutational analyses in toxin binding, in which they play a major role.

In addition to the residues on KcsA, many of the charybdotoxin residues that directly contact KcsA in the complex structure (see Figure 5) have also been previously found to be important for high-affinity binding to potassium channels (*23*, *32*). For example, specific mutations of N30′ and R25′ (both of which exhibit NOE contacts to KcsA) result in 1000-fold decreases in affinity for the *Shaker* K^+ channel, highlighting the importance of electrostatic interactions with D64 residues on the channel. Furthermore, specific mutations of M29′ and Y36′ (which are in van der Waals contact with Y82 of KcsA) and K27′ (which inserts directly into the channel pore) dramatically decrease binding affinity (*23*). Mutations of F2′, W14′, and S37′ (which also make NOE contact with the channel) exhibit only modest decreases in affinity (3−6-fold). In addition, a mutation in K11′ [which forms an additional salt bridge with D64(B) of KcsA] leads to a 5-fold decrease in affinity. The modest decreases in affinity upon mutation of these residues suggest that the interactions observed in the structure may play a larger role in modulating the specificity rather than the potency of binding of charybdotoxin to ion channels. Three additional residues (S10′, T23′, and R34′) have been implicated in binding of charybdotoxin to the *Shaker* K^+ channel through mutational analyses (*23*, *32*). In the KcsA−charybdotoxin complex, both S10′ and R34′ are in van der Waals contact with KcsA and thus may contribute directly to the binding interaction. T23′, however, does not directly contact KcsA, and the decrease in binding affinity observed in binding to the *Shaker* K^+ channel upon mutation of this residue to an aspartic acid (*23*) most likely involves long-range electrostatic effects or changes in the toxin structure.

From an analysis of double mutant cycles, in which sets of amino acids on both the toxin and the channel are mutated and binding affinities measured, several groups have derived thermodynamic couplings between specific amino acid pairs from which distance restraints can be derived (*25*, *29*, *33*, *34*). On the basis of these data, models for charybdotoxin complexed to Kv1.3 (*35*), BgK complexed to Kv1.1 (*33*), and agitoxin 2 (AgTx2) complexed to the *Shaker* K^+ channel (*25*) have been proposed. Given the high degree of homology between agitoxin 2 and charybdotoxin (see Figure 1), we can compare the NMR-derived solution structure described here to the models proposed for agitoxin 2. Interestingly, in the model of the agitoxin−*Shaker* complex, multiple binding modes of the toxin could satisfy the distance restraints derived from thermodynamic mutant cycles, most likely due to intrinsic limitations of the set of coupling constants used in the analysis (*25*). However, of the 10 distance restraints used in the agitoxin analysis (*25*), eight of the homologous amino acid pairs are in van der Waals contact in the solution structure of the KcsA−charybdotoxin complex described here. A subset of three of these restraints has also been used in the docking of charybdotoxin to Kv1.3 (*29*). Only two pairings derived from the coupled mutational data are inconsistent with the NMR structure. A close contact (<3.5 Å) between S11 of AgTx2 (corresponding to S10′ of charybdotoxin) and D431 of *Shaker* (corresponding to D64 of KcsA) was predicted on the basis of the mutant cycle data, but these residues are separated by more than 6 Å in the NMR structure. Significantly, the authors themselves recognized the inability to satisfy this restraint and removed it early in the modeling analysis (*25*). G10 of AgTx2 (corresponding to T9′ of charybdotoxin) and T449 of *Shaker* (corresponding to Y82 of KcsA) were also predicted to be in direct contact (<4 Å). These residues are also separated by more than 6 Å in the NMR structure. Similarly, Rauer et al. used three sets of docking restraints to dock charybdotoxin to Kv1.3 (*35*). One of the three restraints is inconsistent with our NMR structure. A close contact (<5.0 Å) between K31 of charybdotoxin and D386 of Kv1.3 (corresponding to D64 of KcsA) was predicted from the mutant cycle data. However, this pair of residues are separated by ∼10 Å in our KcsA−charybdotoxin complex. Thus, while many of the couplings derived from the double mutant cycles correspond in fact to direct contacts between the residue pairs, other effects produced by the mutations (e.g., conformational changes, long-range electrostatic effects, etc.) can alter the binding affinity and complicate the interpretation of the mutant cycle data.

CONCLUSIONS

Understanding the structural basis of binding of ligand to K^+ channels is critical in investigating the fundamental role that these proteins play in cellular function and in the development of safe and effective therapeutics that interact with these targets. In this study, we determined the solution structure of charybdotoxin bound to the extracellular pore of KcsA. These data provide the first direct structural information about an ion channel complexed to a peptide antagonist, and provide a structural basis for interpreting many of the mutational analyses and modeling studies of these protein−protein complexes. This work can also be extended to study the binding of druglike molecules to this important class of membrane proteins. This would open up the possibility of structure-based drug design on K^+ channel modulators.

SUPPORTING INFORMATION AVAILABLE

A table of structural statistics for the complex, a $^{13}C-^{1}H$SQC spectrum of the methyl groups of KcsA with assignments, a $^{13}C-^{1}H$SQC spectrum of an alanine-labeled sampled showing incorporation of the label, and a stereoview of the backbone atoms (N, Cα, and C′) of 10 NMR-derived structures of the KcsA−charybdotoxin complex when superimposed upon all the backbone atoms in the complex. This material is available free of charge via the Internet at http://pubs.acs.org.

REFERENCES

1. Shieh, C.-C., Coghlan, M., Sullivan, J. P., and Gopalakrishnan, M. (2000) Potassium Channels: Molecular Defects, Diseases, and Therapeutic Opportunities, *Pharmacol. Rev. 52*, 557−593.
2. Doyle, D. A., Cabral, J. M., Pfuetzner, R. A., Kuo, A., Gulbis, J. M., Cohen, S. L., Chait, B. T., and MacKinnon, R. (1998) The Structure of the Potassium Channel: Molecular Basis of K^+ Conduction and Selectivity, *Science 280*, 69−77.
3. Jiang, Y., Lee, A., Chen, J., Cadene, M., Chait, B. T., and MacKinnon, R. (2002) Crystal Structure and Mechanism of a Calcium-gated Potassium Channel, *Nature 417*, 515−522.
4. Jiang, Y., Lee, A., Chen, J., Ruta, V., Cadene, M., Chait, B. T., and MacKinnon, R. (2003) X-ray Structure of a Voltage-Dependent K^+ Channel, *Nature 423*, 33−41.
5. Kuo, A., Gulbis, J. M., Antcliff, J. F., Rahman, T., Lowe, E. D., Zimmer, J., Cuthbertson, J., Ashcroft, F. M., Ezaki, T., and Doyle, D. A. (2003) Crystal Structure of the Potassium Channel KirBac1.1 in the Closed State, *Science 300*, 1922−1926.
6. Jiang, Y., Lee, A., Chen, J., Cadene, M., Chait, B. T., and MacKinnon, R. (2002) The Open Pore Conformation of Potassium Channels, *Nature 417*, 523−526.
7. Roosild, T. P., Greenwald, J., Vega, M., Castronovo, S., Riek, R., and Choe, S. (2005) NMR structure of Mistic, a membrane-integrating protein for membrane protein expression, *Science 307*, 1317−1321.
8. Howell, S. C., Mesleh, M. F., and Opella, S. J. (2005) NMR structure determination of a membrane protein with two transmembrane helices in micelles: MerF of the bacterial mercury detoxification system, *Biochemistry 44*, 5196−206.
9. Oxenoid, K., Kim, H. J., Jacob, J., Sonnichsen, F. D., and Sanders, C. R. (2004) NMR assignments for a helical 40 kDa membrane protein, *J. Am. Chem. Soc. 126*, 5048−5049.
10. Tian, C., Breyer, R. M., Kim, H. J., Karra, M. D., Friedman, D. B., Karpay, A., and Sanders, C. R. (2005) Solution NMR spectroscopy of the human vasopressin V2 receptor, a G protein-coupled receptor, *J. Am. Chem. Soc. 127*, 8010−8011.
11. Williams, K. A., Farrow, N. A., Deber, C. M., and Kay, L. E. (1996) Structure and dynamics of bacteriophage IKe major coat protein in MPG micelles by solution NMR, *Biochemistry 35*, 5145−5157.
12. Medek, A., Olejniczak, E. T., Meadows, R. P., and Fesik, S. W. (2000) An Approach for High-Throughput Structure Determination of Proteins by NMR Spectroscopy, *J. Biomol. NMR 18*, 229−238.
13. Pellechia, M., Meininger, D., Dong, Q., Chang, E., Jack, R., and Sem, D. S. (2002) NMR-Based Structural Characterization of Large Protein−Ligand Interactions, *J. Biomol. NMR 22*, 165−173.
14. Gross, J. D., Gelev, V. M., and Wagner, G. (2003) A sensitive and robust method for obtaining intermolecular NOEs between side chains in large proteins, *J. Biomol. NMR 25*, 235−242.
15. Heginbotham, L., Odessey, E., and Miller, C. (1997) Tetrameric stoichiometry of a prokaryotic K^+ channel, *Biochemistry 36*, 10335−10342.
16. Brunger, A. T., Adams, P. D., Clore, G. M., DeLano, W. L., Gros, P., Grosse-Kunstleve, R. W., Jiang, J. S., Kuszewski, J., Nilges, M., Pannu, N. S., Read, R. J., Rice, L. M., Simonson, T., and Warren, G. L. (1998) Crystallography & NMR system: A new software suite for macromolecular structure determination, *Acta Crystallogr. D54* (Part 5), 905−921.
17. Dominguez, C., Boelens, R., and Bonvin, A. M. (2003) HADDOCK: A protein−protein docking approach based on biochemical or biophysical information, *J. Am. Chem. Soc. 125*, 1731−1737.
18. Bontems, F., Roumestand, C., Gilquin, B., Menez, A., and Toma, F. (1991) Refined structure of charybdotoxin: Common motifs in scorpion toxins and insect defensins, *Science 254*, 1521−1523.
19. MacKinnon, R., Cohen, S. L., Kuo, A., Lee, A., and Chait, B. T. (1998) Structural Conservation in Prokaryotic and Eukaryotic Potassium Channels, *Science 280*, 106−109.
20. Mitcheson, J. S., Chen, J., Lin, M., Culberson, C., and Sanguinetti, M. C. (2000) A Strcutural Basis for Drug-Indiced Long QT Syndrome, *Proc. Natl. Acad. Sci. U.S.A. 97*, 12329−12333.
21. Gulbis, J. M., and Doyle, D. A. (2004) Potassium channel structures: Do they conform? *Curr. Opin. Struct. Biol. 14*, 440−446.
22. Heginbotham, L., LeMasurier, M., Kolmakova-Partensky, L., and Miller, C. (1999) Single streptomyces lividans K^+ channels: Functional asymmetries and sidedness of proton activation, *J. Gen. Physiol. 114*, 551−560.
23. Goldstein, S. A. N., Pheasant, D. J., and Miller, C. (1994) The Charybdotoxin Receptor of a Shaker K^+ Channel: Peptide and Channel Residues Mediating Molecular Recognition, *Neuron 12*, 1377−1388.
24. Ranganathan, R., Lewis, J. H., and MacKinnon, R. (1996) Spatial Localization of the K^+ Channel Selectoivity Filter by Mutant Cycle-Based Structure Analysis, *Neuron 16*, 131−139.
25. Eriksson, M. A. L., and Roux, B. (2002) Modelling the Structure of Agitoxin in Complex with Shaker K^+ Channel: A Computational Approach Based on Experimental Distance Restraints Extracted from Thermodynamic Mutant Cycles, *Biophys. J. 83*, 2595−2609.
26. Korolkova, Y. V., Tseng, G. N., and Grishin, E. V. (2004) Unique interaction of scorpion toxins with the hERG channel, *J. Mol. Recognit. 17*, 209−217.
27. Takeuchi, K., Yokogawa, M., Matsuda, T., Sugai, M., Kawano, S., Kohno, T., Nakamura, H., Takahashi, H., and Shimada, I. (2003) Structural Basis of the KcsA K^+ Channel and Agitoxin2 Pore-Blocking Toxin Interaction by Using the Transferred Cross-Saturation Method, *Structure 11*, 1381−1392.
28. Fu, W., Cui, M., Briggs, J. M., Huang, X., Xiong, B., Zhang, Y., Luo, X., Shen, J., Ji, R., Jiang, H., and Chen, K. (2002) Brownian Dynamics Simulations of the Recognition of the Scorpion Toxin Maurotoxin with the Voltage-Gated Potassium Ion Channels, *Biophys. J. 83*, 2370−2385.
29. Gao, Y.-D., and Garcia, M. L. (2003) Interaction of Agitoxin2, Charybdotoxin, and Iberiotoxin with Potassium Channels: Selectivity between Voltage-Gated and Maxi-K Channels, *Proteins: Struct., Funct., Genet. 52*, 146−154.
30. Lipkind, G. M., and Fozzard, H. A. (1997) A model of scorpion toxin binding to voltage-gated K^+ channels, *J. Membr. Biol. 158*, 187−196.
31. Goldstein, S. A., and Miller, C. (1992) A point mutation in a Shaker K^+ channel changes its charybdotoxin binding site from low to high affinity, *Biophys. J. 62*, 5−7.
32. Stampe, P., Kolmakova-Partensky, L., and Miller, C. (1994) Intimations of K^+ channel structure from a complete functional map of the molecular surface of charybdotoxin, *Biochemistry 33*, 443−450.

33. Gilquin, B., Racape, J., Wrisch, A., Visan, V., Lecoq, A., Grissmer, S., Menez, A., and Gasparini, S. (2002) Structure of the BgK−Kv1.1 complex based on distance restraints identified by double mutant cycles. Molecular basis for convergent evolution of Kv1 channel blockers, *J. Biol. Chem. 277*, 37406−37413.
34. Imredy, J. P., and MacKinnon, R. (2000) Energetic and structural interactions between δ-dendrotoxin and a voltage-gated potassium channel, *J. Mol. Biol. 296*, 1283−1294.
35. Rauer, H., Lanigan, M. D., Pennington, M. W., Aiyar, J., Ghanshani, S., Cahalan, M. D., Norton, R. S., and Chandy, K. G. (2000) Structure-guided transformation of charybdotoxin yields an analog that selectively targets Ca^{2+}-activated over voltage-gated K^+ channels, *J. Biol. Chem. 275*, 1201−1208.

BI051656D